Prediction of Fire Growth for Compartments of Office Buildings as Part of a Fire Risk/Cost Assessment Model

GEORGE HADJISOPHOCLEOUS* AND ZHUMAN FU
Department of Civil and Environmental Engineering
Carleton University, Ottawa, ON, K1S 5B6, Canada

SIMON FU AND CHARLES DUTCHER
Public Works and Government Services Canada
Ottawa, ON, Canada

ABSTRACT: This article presents a zone model for the prediction of fire growth in a commercial compartment of an office building as part of a fire risk and cost assessment software package. The model developed is a combination of a transient, two-zone submodel used for the pre-flashover fire state and a quasi-steady, single-zone submodel for the post-flashover state. In the two-zone submodel, the selected four independent governing variables are pressure, enthalpy of the upper layer, and the masses of the upper and lower layers. To determine the conditions in the fire compartment, the model considers combustion, fluid flow, and heat transfer. The single-zone submodel includes the energy balance equation, and equations of energy losses due to smoke flow, conduction through the compartment walls, and radiation. The article also presents results of model validation using experimental data from tests in a standard room and in an experimental atrium with a smoke exhaust system. Comparisons of smoke, temperature, interface height and smoke flow rates have been conducted. For the data comparison, the differences between experimental and predicted results range from 2 to 16%.

KEY WORDS: risk assessment, fire growth, zone modeling.

INTRODUCTION

A COMPUTER PROGRAM for risk assessment called FiRECAM (fire risk evaluation and cost assessment model) has been developed by the

*E-mail: george_hadjisophocleous@carleton.ca

1042-3915/07/03 0185–25 $10.00/0 DOI: 10.1177/1042391507069336

National Research Council of Canada (NRCC) with Public Works and Government Services Canada (PWGSC) [1]. This model can be used to identify cost-effective fire safety designs of apartment and office buildings to meet the safety requirements of the National Building Code of Canada [2]. FiRECAM consists of a number of submodels that simulate the dynamic interaction of fire growth, smoke movement, occupant response and evacuation, and fire department intervention. The current fire growth model of FiRECAM is a one-zone model [3], which calculates the burning rate, temperature, and the production and concentration of toxic gases as a function of time for the fire room. To use FiRECAM for office buildings with commercial floors or with an atrium, a new fire growth model is required capable of handling the two zones expected in the atrium and the commercial compartments before flashover, as well as the post-flashover conditions in the commercial compartments. In this case, a commercial compartment in an office building refers to compartments in office buildings that are on floors used for retail services. The use of fluid dynamic models that involve thousands of computational cells was ruled out due to the calculation time requirements that make this technique not suitable for risk modeling calculations.

To predict fire growth in a commercial or atrium compartment of an office building, a model was developed at Carleton University that uses the two-zone modeling approach for the pre-flashover fire and the single-zone modeling approach for the post-flashover fire. The basic approaches of the two-zone modeling part can be found in [4], and the approaches for the one-zone modeling part can be found in [5].

This article describes the governing equations of the two-zone and single-zone submodels and the numerical methods used to solve the set of governing equations of each submodel. A description is also given for the various modules used to handle combustion, heat transfer, and fluid flow.

The article also presents results of model validation in which experimental data from tests for a standard room and an experimental atrium with a smoke exhaust system were used for comparisons with the predictions of the model.

TWO-ZONE MODELING OF PRE-FLASHOVER FIRE

In two-zone modeling, the gas within a compartment is divided into two zones. Within each zone, the physical parameters such as gas temperature and species concentrations are assumed to be spatially uniform. From the mass and energy conservation and ideal gas law, a set of ordinary differential equations can be derived. In such a model, the physical details of the gas within a zone are not considered, while mass and energy transport

between zones is calculated by modeling the relevant fire subprocesses of combustion, fluid flow, and heat transfer. A number of models of this type have been developed, and references [6,7] give a comprehensive review of existing fire models.

For two-zone modeling, four independent solution variables are needed. There are various combinations for selecting these variables. For the general derivation of these equations and their numerical characteristics, please refer [4,8,9]. In this model, the selected solution variables are pressure P, upper layer enthalpy H_U, upper layer mass m_U, and lower layer mass m_L. The governing equations set is as follows:

$$\frac{dP}{dt} = \frac{\gamma - 1}{V}(\dot{S}_U + \dot{S}_L) \tag{1}$$

$$\frac{dH_U}{dt} = \dot{S}_U + V_U \frac{dP}{dt} \tag{2}$$

$$\frac{dm_U}{dt} = \dot{\Omega}_U \tag{3}$$

$$\frac{dm_L}{dt} = \dot{\Omega}_L \tag{4}$$

where, $\dot{\Omega}_i$ is the net mass gain rate of layer i by mass flow through its boundary as a source term, and $\dot{S}_i$ is the net energy gain rate of layer i as a source term. V is the total volume of the compartment. γ is the ratio of specific heats for air. The derivation of the above equations can be found in [4].

In the above governing equations, the mass and energy source terms, $\dot{\Omega}_i$ and $\dot{S}_i$, are obtained by modeling the relevant fire subprocesses, including combustion, fluid flow, and heat transfer. The following sections present more details of modeling these processes.

Combustion

Heat Release Rate

Heat release rate is calculated based on the available oxygen for combustion in the fire plume. First, a nominal heat release rate Q_N is specified using a t^2 fire growth rate as follows:

$$Q_N = \min(\alpha t^2, Q_{Nmax}) \tag{5}$$

where, α is the coefficient of the t^2 fire; t is the elapsed time; Q_{Nmax} is the specified maximum heat release rate. The reason for using t^2 fires is to make the model consistent with other submodels of the risk model FiRECAM. The use of t^2 fires in design applications is described in [10,11].

The available oxygen is calculated through the equivalence ratio in the plume ϕ, and then the real heat release rate Q is obtained as follows [4]:

$$Q = \frac{Q_N}{\max(\phi,1)} \tag{6}$$

The equivalence ratio ϕ is defined as

$$\phi = \frac{Q_N}{(\Delta H)_O \dot{m}_e Y_{O_2} C_{LOL}} \tag{7}$$

where $(\Delta H)_O$ is the heat of combustion per unit mass of oxygen; $\dot{m}_e$ is the mass entrainment rate of the plume, the calculation of which is discussed later; Y_{O_2} is the oxygen mass fraction; and C_{LOL} is the lower oxygen limiting coefficient.

Combustion Chemistry

In this model, the global combustion chemistry is written as follows:

$$m_{PF} + m_{O_2} \rightarrow m_{PF\,min} + m_{TUCF} + m_{CO_2} + m_{CO} + m_{soot} + m_{H_2O} \tag{8}$$

where, m_{PF} is the mass of the pyrolyzed fuel, obtained from nominal heat release rate divided by heat of combustion; m_{O_2} is the mass consumption of oxygen; m_{PFmin} is the mass of the incombustible minimal part of the pyrolyzed mass m_{PF}; m_{TUCF} is the mass production of the total unburned combustible fuel; m_{CO_2}, m_{CO}, m_{soot}, and m_{H_2O} are the mass productions of carbon dioxide, carbon monoxide, soot, and water, respectively.

The pyrolyzed mass m_{PF} is assumed to be composed of two parts: the combustible main part and the noncombustible, minimal part, m_{PFmin}. The main part is the mass of the elements C, H, and O of the pyrolyzed fuel. The noncombustible part, m_{PFmin}, can be any minimal components, having a mass much less than the total fuel mass, that is assumed not to be involved in the further combustion process. Thus, m_{PFmin} from m_{PF} in the left side of Equation (8) directly goes into its right side.

More details on the combustion model can be found in [4].

Fluid Flow

Plume Entrainment

As the fire plume rises from the fire area towards the ceiling, it entrains air. There are a number of empirical correlations that can be used to calculate air entrainment. However, full-scale standard room fire tests at

National Institute of Standards and Technology (NIST) indicate that McCaffrey's model gives the best agreement with the measured entrainment rates, as discussed in [12]. In this model, McCaffrey's entrainment model is used [13]:

$$\frac{\dot{m}_e}{Q} = C_{E1}\left(\frac{Z_e}{Q^{2/5}}\right)^{C_{E2}} \tag{9}$$

where $\dot{m}_e$ is the plume entrainment rate; Z_e is the interface height from the burning surface; Q is the heat release rate; C_{E1} and C_{E2} are constant coefficients as follows:

$$\text{if} \quad 0 \le \frac{Z_e}{Q^{2/5}} < 0.08, \quad C_{E1} = 0.011, \quad C_{E2} = 0.566$$

$$\text{if} \quad 0.08 \le \frac{Z_e}{Q^{2/5}} < 0.20, \qquad C_{E1} = 0.026, \quad C_{E2} = 0.909$$

$$\text{if} \quad 0.20 \le \frac{Z_e}{Q^{2/5}}, \quad C_{E1} = 0.124, \quad C_{E2} = 1.895$$

Equation (9) is for fires burning at a place away from walls. If fires burn along the walls or in corners, plume entrainment rate will be restricted. In this case, the equation will be adjusted as follows [14]:

$$\frac{\dot{m}_e}{Q} = C_{E1}\left(\frac{Z_e}{(\omega Q)^{2/5}}\right)^{C_{E2}} \tag{10}$$

where, ω is 4 for a corner fire, and 2 for a wall fire.

Door/Window Vent Flow

Mass flow through a vertical vent such as a door or window is driven by the pressure difference between the two sides of the vent, and it can be calculated by integrating Bernoulli's equation along the vertical direction of the vent. In this model, it is assumed that the vent is rectangular. To calculate the flow rate, the vertical integral limit from sill to soffit needs to be divided into several parts, each part having the same flow direction. Then for each such division, the following formula from Bernoulli's equation can be obtained. More details can be found in [15].

$$\dot{m}_V = \frac{2}{3} C_V A_V \sqrt{2\rho}\left(\frac{|P_t| + \sqrt{|P_t||P_b|} + |P_b|}{\sqrt{|P_t|} + \sqrt{|P_b|}}\right) \tag{11}$$

where $\dot{m}_V$ is the mass flow rate through this part of the vent; P_t and P_b are the pressure differences at the top and bottom positions of this division; ρ is the gas density of source side; A_V is the area of this part of vent; and C_V is the coefficient of vent flow.

Ceiling Vent Flow

Vertical airflow through a ceiling vent involves two flow-driving forces, buoyancy, and pressure. It is not appropriate to directly use Bernoulli's equation for the ceiling vent flow because in addition to pressure difference, buoyant force contributes to the flow, which may lead to bi-directional exchange flow. Cooper et al. [16] developed a calculation model for unstable flow through shallow, horizontal, circular vents under high Grashof number condition, which is the case encountered in a building fire. This method will first determine whether a bi-directional flow exists, then the flow from the higher-pressure side to the lower-pressure side V_H, flow from the lower pressure to the higher side V_L and the net flow rate V_N will be calculated accordingly. The three flow rates have the following relation:

$$V_H = V_L + V_N \tag{12}$$

The equations for calculating these flow rates can be found in [16].

Mechanical Ventilation

Mechanical ventilation is normally used in an atrium area of a building to extract smoke to the outside in order to keep the smoke height at a specified level. In such a system, an exhaust fan is an essential part. Thus, in this model, a simple mechanical ventilation model is implemented, providing two options. The first option allows the user to specify a constant volume flow rate and the second option provides the user with the flexibility to input fan performance data as well as the pressure drop of the exhaust system. The model calculates the actual flow rate based on the real pressure developed in the atrium in the course of the fire. The second option provides a more realistic prediction of the performance of the exhaust system than the first. Each fan has a performance curve or table indicating the performance of the fan, i.e., its volumetric flow rate as a function of the total pressure [17]. In this model, the user is allowed to input a number of points of the curve; then for any point between two neighboring input points, linear interpolation is used to obtain the needed data.

It is possible for a fan to both extract upper layer smoke and lower layer air to the outside. For this case, an approach has been used in the two-zone

model to identify how much gas is extracted from each zone. The details can be found in [4].

Heat Transfer

Conduction

To calculate conduction heat transfer through the compartment boundaries, a 1D conduction model is used. The governing equation is as follows:

$$\frac{\partial T}{\partial t} = \frac{K}{\rho C}\frac{\partial^2 T}{\partial x^2} \tag{13}$$

For both surfaces of each boundary, convection and radiation heat fluxes are calculated and used as boundary conditions.

Convection for Lower Wall or Floor

The lower wall is defined as the lower part of the wall, which is in contact with the lower layer. Convection heat transfer for a lower wall or floor is calculated using the following equation:

$$Q_{\text{conv}} = hA_{\text{w}}\left(T_{\text{g}} - T_{\text{w}}\right) \tag{14}$$

where, Q_{conv} is the convection heat loss to a surface of a wall or floor; A_{w} is the heat transfer area; T_{g} is the temperature of gas; T_{w} is the temperature of the surface of a wall or floor; h is the convection heat transfer coefficient. The coefficient h is different for a wall or a floor due to their different geometrical orientation. It is calculated using nondimensional correlations between the Nusselt, Prandtl, and Grashof numbers, which can be found in [18,19].

Convection for Ceiling and Upper Wall

In the fire room, ceiling jet-induced convection heat transfer should be separately evaluated due to its specific magnitude. Heat loss due to the ceiling jet can be calculated using the following formula:

$$Q_{\text{ceil}} = \int_A h(T_{\text{ad}} - T_{\text{ceil}})\,\mathrm{d}A \tag{15}$$

where Q_{ceil} is the gas heat loss through the ceiling surface; h is the heat transfer coefficient; T_{ad} and T_{ceil} are characteristic gas and ceiling surface temperatures, which are obtained from NIST's correlations [20,21]. In this calculation, the ceiling surface is converted into an equivalent circular

surface with the same area, and the plume impingement point is assumed to be at the center of the surface. The ceiling surface temperature is assumed to be spatially uniform. Heat convection for the upper wall is separately calculated using a simple method the details of which can be found in [4].

Radiation

A two-surface radiation heat transfer model is used in this model. One surface represents the surface of the ceiling and upper wall surface in contact with the smoke layer. The other surface represents the floor and lower wall surface in contact with the lower layer. In order to simplify the calculation process, the flame is assumed to be a sphere with its center located at half the flame height measured from the fuel bed. Additionally, the sphere is assumed to be the third differential emitting blackbody surface interacting with the upper surface, lower surface, and upper layer gas. The smoke layer is considered to be an absorptive medium and the lower layer is considered to be transparent. The detailed equations can be found in [4].

SINGLE-ZONE MODELING OF POST-FLASHOVER FIRE

The post-flashover stage of fire is modeled using a single-zone model in which the gas within the compartment is taken as a well-stirred zone with spatially uniform physical or chemical properties. The one-zone model for post-flashover fire includes the equations for energy balance as well as energy losses due to smoke flow, conduction through the compartment walls, and radiation.

This submodel is based on a quasi-steady, single-zone model for post-flashover fires described in [5]. It is assumed that the heat release rate of the fuel is balanced by the heat loss due to smoke outflow, wall losses, and window radiation losses. The basic heat balance equation is as follows:

$$Q = C_P \dot{m}_f (T_f - T_{amb}) + Q_W + Q_R \tag{16}$$

where Q is the heat release rate; C_P is the heat capacity at constant pressure; $\dot{m}_f$ is the mass outflow rate; T_f and T_{amb} are the temperatures of smoke and the ambient; Q_W and Q_R are wall loss and window radiation loss.

Heat release rate Q is evaluated as follows:

$$Q = b_P \min\left(Q_N, \dot{m}_{air} Y_{O_2} \Delta H_O\right) \tag{17}$$

where b_P is a constant combustion efficiency; $\dot{m}_{air}$ is the air flow rate, which is calculated using the following equation from [5] by ignoring the difference of molecular weights of smoke and air:

$$\dot{m}_{air} = \frac{2}{3} C_V \rho_0 \left[2g \frac{1 - (T_{amb}/T_f)}{\left(1 + \left[(1 + (\dot{m}_{PF}/\dot{m}_{air}))^2 (T_f/T_{amb})\right]^{1/3}\right)^3} \right]^{1/2} A_V \sqrt{H_V} \quad (18)$$

where, ρ_0 is the density of the ambient air; H_V is the height of the opening.

The wall loss term and the window radiation loss term can both be expressed as a function of the smoke temperature and wall surface temperature, and the wall surface temperature can be obtained by solving Equation (13) for heat conduction through the wall. The details of these equations can be found in [5]. Equation (16) is converted to a nonlinear algebraic equation with its unknown solution variable being smoke temperature T_f.

Furthermore, when switching from the pre-flashover two-zone submodel to the post-flashover one-zone submodel, the temperature and species concentrations of the upper layer and the thermal properties and temperature profile of the upper wall of the two-zone submodel are taken as the initial values of the one-zone submodel. The switching criterion for flashover in this model is taken as 600°C. In this case, some extra energy is created when switching; however, it is assumed that this can be ignored under a flashover condition.

The model also considers the decay stage of the fire after flashover during which the burning rate of a fire decreases because the fuel is consumed. The heat release rate of decay is estimated using the following equation:

$$Q(t) = \left(1 - 1.75 \frac{(t - t_{od})}{t_{fb}}\right) Q_{max} \quad (19)$$

where t_{od} is the time of onset of the decay phase, when 80% fuel is consumed; t_{fb} is the duration of fully developed burning; Q_{max} is the heat release rate during fully developed burning phase.

NUMERICAL METHOD

One significant property of the equation set of two-zone modeling is its stiffness due to the presence of multiple time scales. Stiffness affects the numerical calculation of the equation set. In fact, this property requires

the application of special numerical solution methods [22,23]. Backward differentiation formulas are generally used to solve the stiff problems. There are a number of solvers available to solve the stiff ordinary differential equation system. In this model, a solver called LSODA, developed by Petzold [24], is used to integrate the equation set numerically. Due to its implicitness, an iteration process composed of prediction and correction is applied. A Newton iterative method is used to speed up the converging process. In this algorithm, the order and time-step size are automatically chosen through estimating local truncation errors.

In addition, there are four source terms to be solved, upper and lower layer mass variation rates $\dot{\Omega}_U$ and $\dot{\Omega}_L$, upper and lower layer energy variation rates $\dot{S}_U$ and $\dot{S}_L$. These four parameters are obtained from the calculation of the relevant fire submodels described earlier. In this model, the tri-diagonal matrix algorithm (TDMA) method was used to numerically solve the 1D heat conduction equation. The ceiling jet-induced convection heat transfer is a problem of 1D definite integral, in which the heat flux has to be integrated over the ceiling surface.

The nonlinear algebraic equation of the single-zone, post-flashover model is solved using the Steffenson acceleration approach [25].

COMPARISON WITH EXPERIMENTAL RESULTS

The developed model was used to simulate full-scale fire experiments conducted in a standard room and in an atrium with mechanical exhaust, and was reported in [26,27]. The predictions of the model are compared with the reported experimental data. These simulations and the comparisons are discussed in this section.

Standard Compartment

Dembsey et al. [26] reported results of a number of fire experiments conducted in a single compartment similar in size, geometry, and construction to the standard fire test room. This compartment has dimensions of $2.5 \times 3.7 \times 2.5\,m^3$, with a single doorway, 0.76 m wide and 2.0 m high, centered on one of the shorter sides. A $0.61 \times 1.22\,m^2$ porous surface burner was placed into the compartment with its porous surface being 0.61 m above the floor. The propane-fired burner supplied heat at a steady rate between 330 and 980 kW for the duration of each experiment. Three sets of experimental data with heat release rates at 330, 630, and 980 kW were compared to two comprehensive compartment fire models, CFAST and FIRST. The developed fire growth model was used to simulate

these tests. The input data of the model are shown in Tables 1–3. The output results are shown in Figures 1–11.

The transient results of the model for these runs are shown in Figures 1–3. Figure 1 presents the predicted smoke temperature with time. The figure shows that the smoke temperature of the case with a fire of 980 kW exceeds 600°C, which is the temperature criterion for flashover assumed in the model. As the figure shows around this point (at about 2.5 min), there is a small fluctuation in the temperature due to the switching from the two-zone model to the one-zone model.

Figure 2 presents the interface heights for the three cases. The figure shows that the curve for the flashover case stops at the flashover time because there is no interface height in the post-flashover single-zone model.

Table 1. Input fuel properties of the two-zone model.

Parameter	Unit	Value
Fuel	N/A	C_3H_8
Heat of combustion	MJ/kg	44
Radiation fraction	N/A	0.27
Heat release rate	kW	330, 630, 980
Simulation time	min	30, 35, 20
Hydrogen fraction	N/A	0.18
Carbon fraction	N/A	0.82

Table 2. Input thermal properties of the compartment boundaries.

	Ceiling	Wall	Floor
Thickness (m)	0.066	0.054	0.044
Density ($kg\,m^{-3}$)	449	449	770
Conductivity ($W\,m^{-1}K^{-1}$)	0.10	0.10	0.14
Specific heat ($J\,kg^{-1}K^{-1}$)	1090	1090	900
Surface emissivity	0.9	0.9	0.9

Table 3. Dimensions of the compartment, door, and burner.

	Depth (m)	Width (m)	Height (m)
Compartment	2.5	3.7	2.5
Door	N/A	0.76	2.0
Burner's surface location	1.25	1.85	0.61

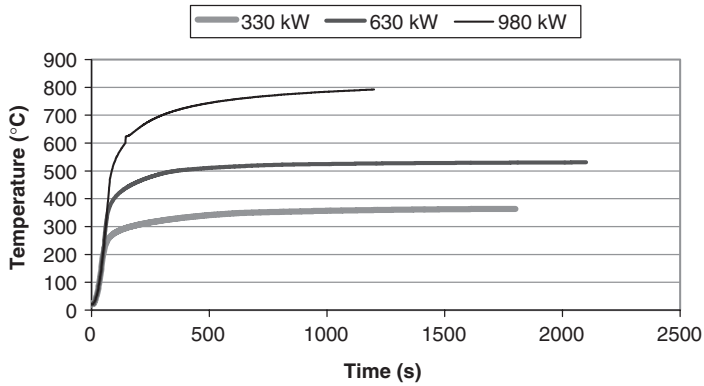

Figure 1. *Smoke temperatures of the three cases at different heat release rates (HRRs).*

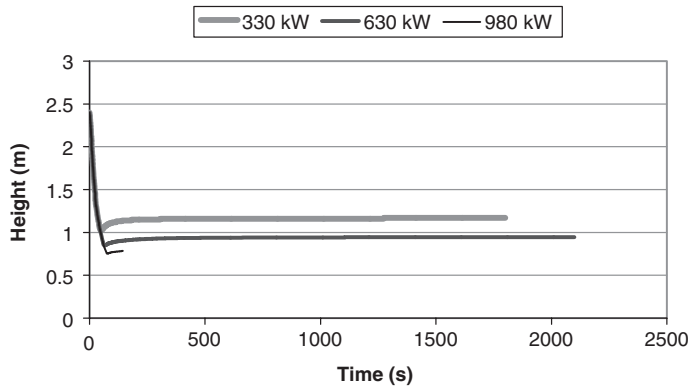

Figure 2. *Smoke interface heights of the three cases at different HRRs.*

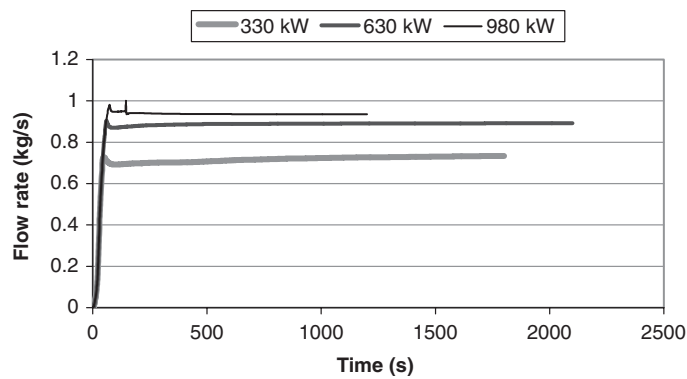

Figure 3. *Smoke flow rates of the three cases at different HRRs.*

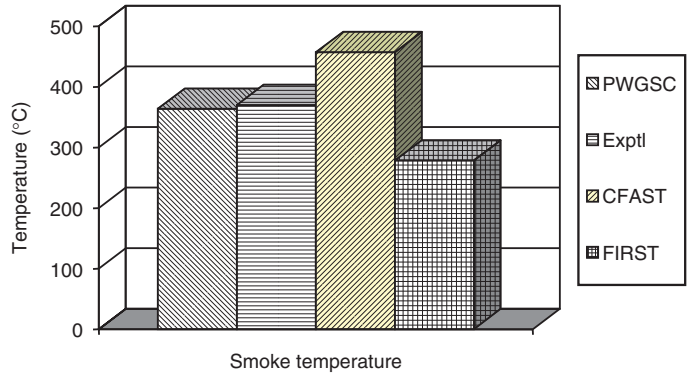

Figure 4. *Smoke temperature of the 330 kW case at 30 min time. The legend symbol, ''Exptl'', represents the experimental result. (The color version of this figure is available online.)*

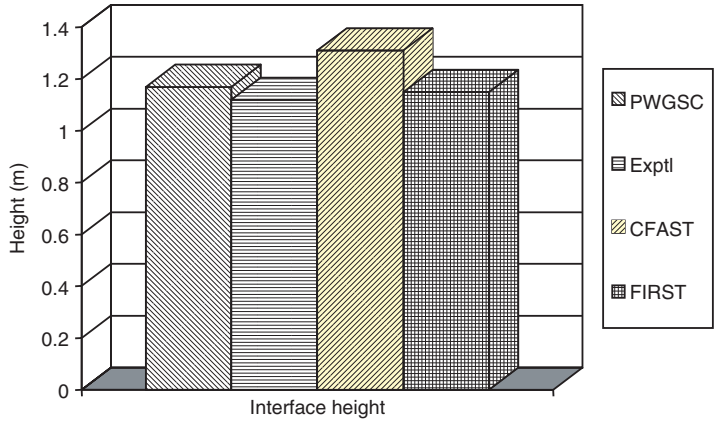

Figure 5. *Smoke interface height of the 330 kW case at 30 min time. (The color version of this figure is available online.)*

Figure 3 depicts the model prediction for the flow rates of smoke out of the door. The fluctuation seen in the curve of the flashover case is a result of the switching from the two-zone to the single-zone model.

Figures 4–6 present comparisons of the predicted results for the case of 330 kW at 30 min. Figure 4 provides a comparison of the predicted smoke layer temperature, the experimental result (denoted as ''exptl'' in the figures), and the predictions of the two-zone models CFAST and FIRST. Figure 5 compares the interface height of the smoke layer and Figure 6 presents a comparison of the mass flow rate of smoke out of the door. It is shown that the model predictions of upper layer temperature, interface height, and vent

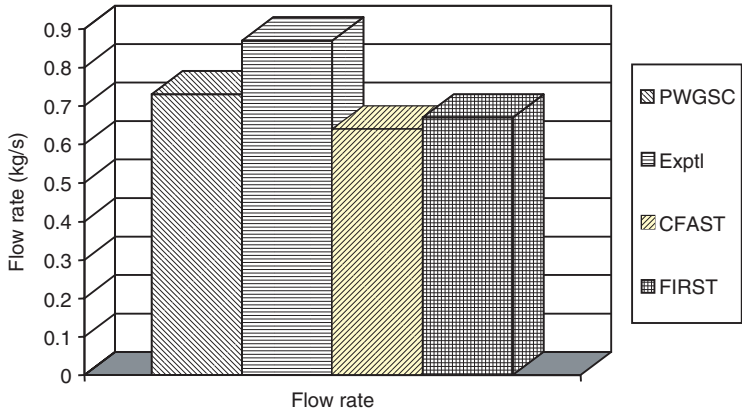

Figure 6. *Smoke flow rate of the 330 kW case at 30 min time. (The color version of this figure is available online.)*

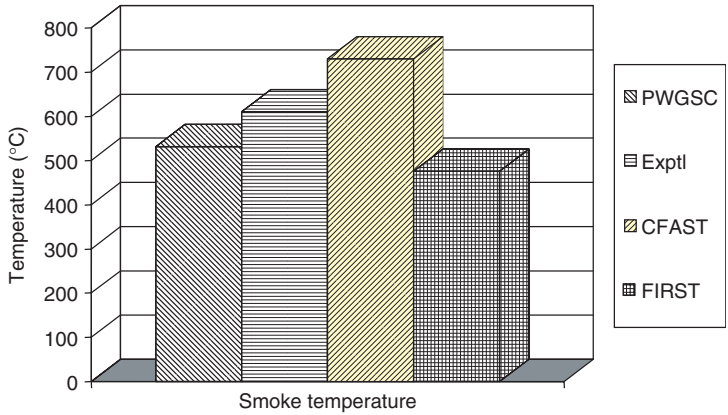

Figure 7. *Smoke temperature of the 630 kW case at 35 min time. (The color version of this figure is available online.)*

flow rate compare favorably with the experimental data, with the differences between predicted and experimental results ranging from 2 to 16%.

Figures 7 to 9 present comparisons of model predictions and experimental data for the case of 630 kW at 35 min. Figure 7 compares the smoke layer temperature, Figure 8 the interface height, and Figure 9 the mass flow rate of smoke out of the door. It is shown from the figures that the results of the model for this case compare well with the experimental data, with the largest difference between predicted and experimental results less than 15%.

Figures 10 and 11 present the comparisons for the case of 980 kW at 20 min. Figure 10 compares the smoke layer temperature and Figure 11

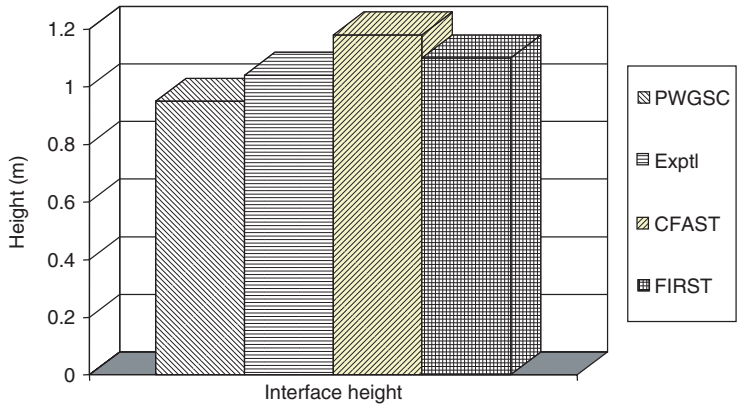

Figure 8. *Smoke interface height of the 630 kW case at 35 min time. (The color version of this figure is available online.)*

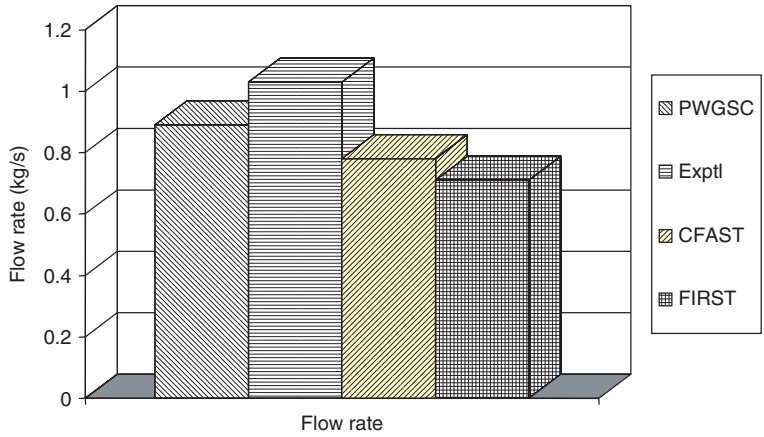

Figure 9. *Smoke flow rate of the 630 kW case at 35 min time. (The color version of this figure is available online.)*

the mass flow rate of smoke out of the door. It is shown that this model gives favorable results for both parameters, with the difference between predicted and experimental results for each parameter less than 10%. As the room of this case has reached flashover, there are no interface height comparisons.

An Experimental Atrium with Mechanical Ventilation

A number of experiments were conducted at NRCC to investigate the effectiveness of the smoke management system of an experimental

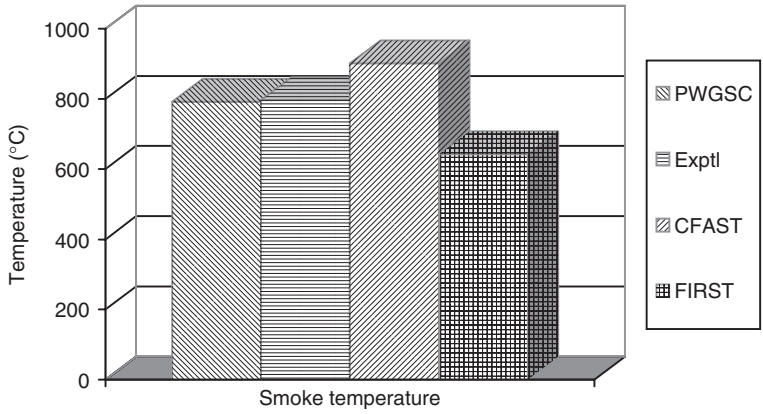

Figure 10. *Smoke temperature of the 980 kW case at 20 min time.*

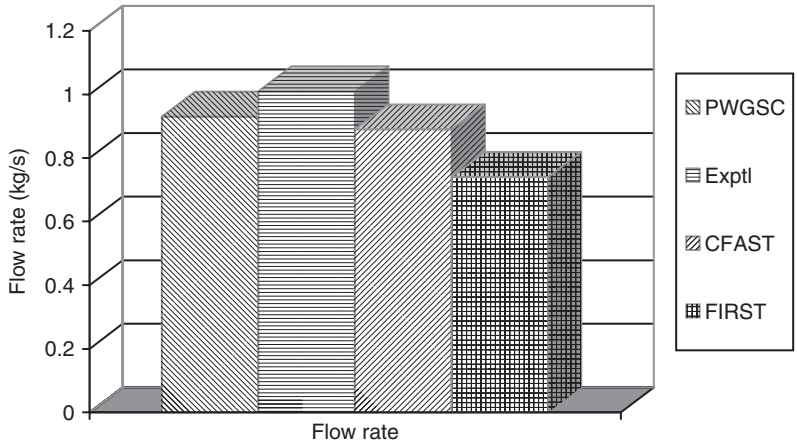

Figure 11. *Smoke flow rate of the 980 kW case at 20 min time.*

atrium [27]. Two sets of data are used for comparisons with the prediction of the developed model.

A schematic diagram of the experimental facility used in that study is shown in Figure 12. The facility is an experimental atrium with dimensions of 9 m × 6 m × 5.5 m in height. The interior wall surface of the compartment was insulated using 25 mm thick rock fiber insulation.

A ventilation system was used to supply fresh air into the compartment through openings in the floor around the walls. These openings had a width of 0.1 m, and a total length of 22.8 m. Inlet air was supplied to the four sides

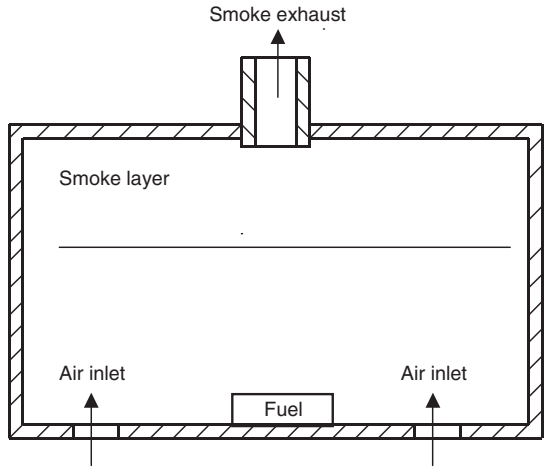

Figure 12. *Schematic of the test facility.*

of the room through a duct system in the under-floor space. Thirty-two exhaust inlets with a diameter of 150 mm were located in the ceiling of the compartment. These inlets were used to extract the hot gases from the compartment during the tests. All exhaust ducts were connected to a central plenum. A 0.6 m diameter duct was used between the plenum and an exhaust fan.

A square propane sand burner was used as the fire source. The burner was capable of simulating fires ranging from 15 to 1000 kW. Twelve CO_2 inlets and 15 thermocouples were located at one of the room quarter points at various heights. The thermocouples, together with the CO_2 measurements, were used to determine the depth of the hot layer in the compartment. The volume flow rate, temperature, CO_2, and oxygen concentrations were measured in the main exhaust duct. These measurements were used to determine the heat release rate of the fire, as well as to calculate the exhaust rate of the ventilation system. A pitot tube and thermocouples, located at the center of the duct, were used to determine the volumetric flow rate in the duct.

The basic input data used in the model are shown in Tables 4–7. It includes fuel properties, thermal properties of the compartment boundaries, the dimensions, initial temperatures, and exhaust rates.

The experimental results, shown in this article, are the hot layer temperatures, interface heights, and hot layer CO_2 concentrations. The interface height is obtained from the concentration profiles based on their maximum gradient. The smoke layer temperature and CO_2 concentration are then calculated by averaging the measured data within the smoke layer.

Table 4. Input fuel properties of the two-zone model.

Fuel	Heat of combustion (MJ/kg)	Radiation fraction	HRR (kW)	χ_H	χ_C
C_3H_8	44	0.27	250, 600	0.18	0.82

Table 5. Input thermal properties of the compartment boundaries.

Thickness (m)	Density ($kg\,m^{-3}$)	Conductivity ($W\,m^{-1}K^{-1}$)	Specific heat ($J\,kg^{-1}K^{-1}$)	Surface emissivity
0.025	130	0.08	900	0.9

Table 6. Dimensions of the compartment, door, and burner.

	Depth (m)	Width (m)	Height (m)
Compartment	9	6	5.5
Floor vent	22.8	0.1	N/A
Burner's surface location	4.5	3.0	0.2

Table 7. Initial temperatures and exhaust rates.

Initial temperature (°C)	Exhaust rate at 250 kW (m^3/S)	Exhaust rate at 600 kW (m^3/S)
24, 26	4.5	4.8

The transient predictions of the model for the hot layer temperature, CO_2 concentration and interface height of the first test are shown in Figures 13–15. It can be seen from these figures that all three parameters gradually approach the steady state.

Comparison with the experimental data for the first test is shown in Figures 16–18. In general, the predicted results using the model are in good agreement with the experimental data. Figure 16 presents the experimental and predicted smoke layer temperatures for the 250 and 600 kW cases. It can be shown that very good agreement has been obtained. Figure 17 shows that the prediction of the smoke layer CO_2 concentration is very agreeable with experimental data. Figure 18 gives the comparison results for the interface heights of the smoke layer. Very favorable results have also been predicted, with the largest difference between predicted and experimental results less than 10%.

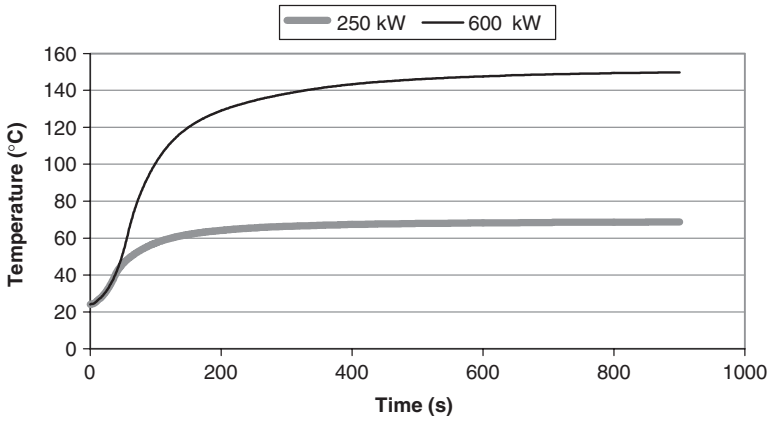

Figure 13. *Transient simulation results for smoke layer temperature.*

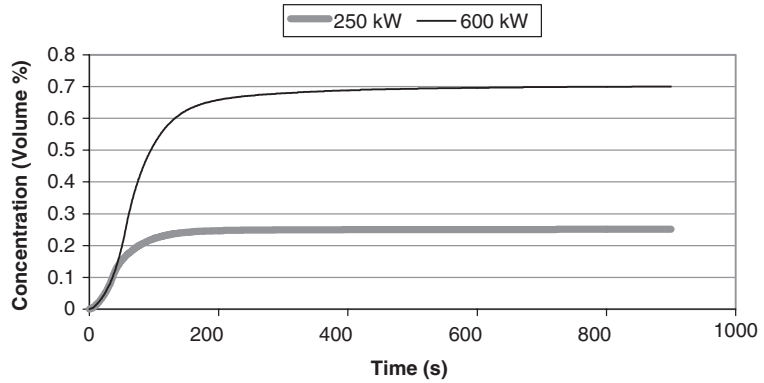

Figure 14. *Transient simulation results for smoke layer CO_2 concentration.*

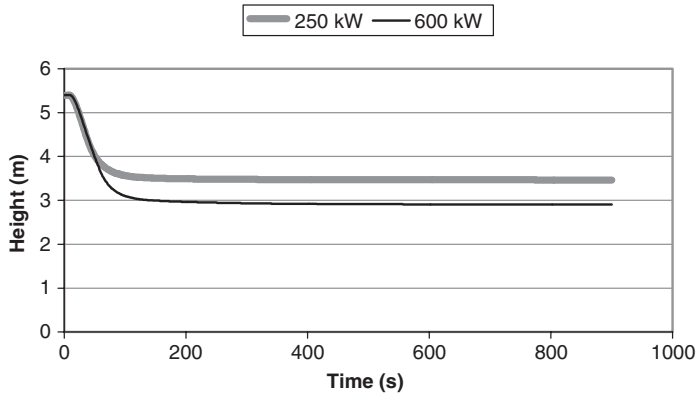

Figure 15. *Transient simulation results for smoke layer interface height.*

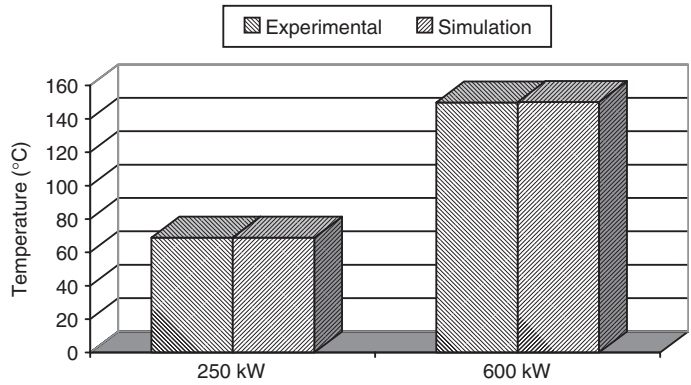

Figure 16. *Experimental and simulation results for smoke layer temperature.*

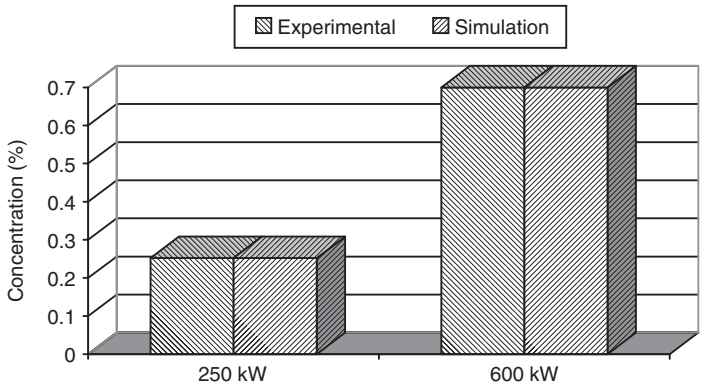

Figure 17. *Experimental and simulation results for smoke layer CO_2 concentrations.*

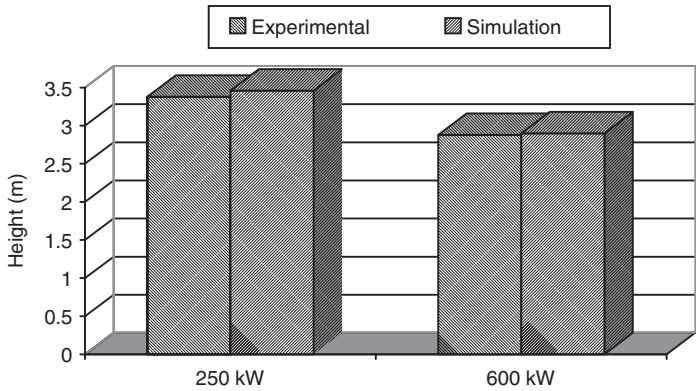

Figure 18. *Experimental and simulation results for smoke layer interface height.*

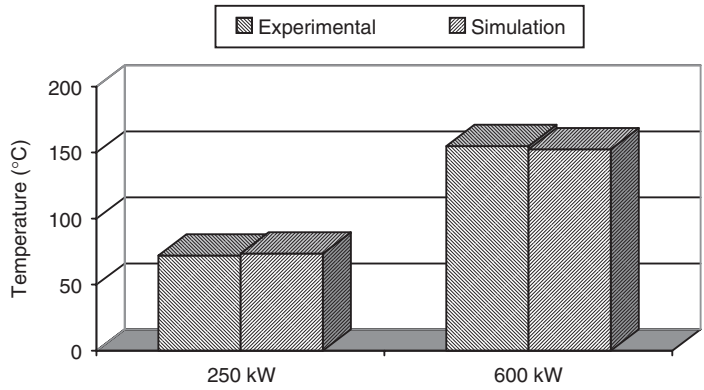

Figure 19. *Experimental and simulation results for smoke layer temperature.*

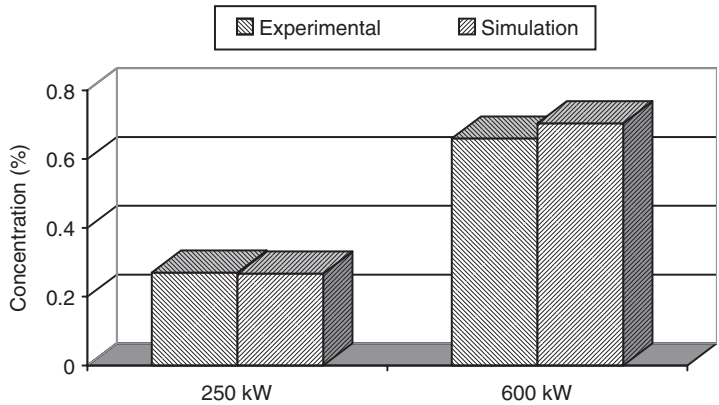

Figure 20. *Experimental and simulation results for smoke layer CO_2 concentration.*

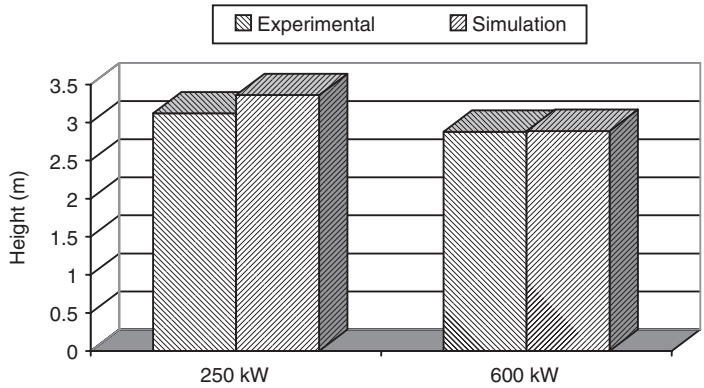

Figure 21. *Experimental and simulation results for smoke layer interface height.*

Experimental data and predicted results for the second test are shown in Figures 19–21. The input data for the two tests are basically the same except for the initial temperature and the extension of the exhaust inlets. Similar to the first test, in general, the predicted results using the model are in good agreement with the experimental data. Figure 19 presents the experimental and predicted smoke layer temperatures. Figure 20 shows that the prediction of the smoke layer CO_2 concentration is in agreement with the experimental data. Figure 21 gives the comparison of results for the interface height of the smoke layer.

CONCLUSIONS

A zone-type fire growth model for the compartment of fire origin has been developed for use in the fire risk evaluation and cost assessment model FiRECAM. Based on the different characteristics of pre- and post-flashover fire phenomena, this model includes a two-zone component computing the fire conditions in the pre-flashover stage and a single-zone submodel for the post-flashover stage. The governing equations of the two-zone submodel are solved using a stiff ordinary differential equation solver LSODA, and the one-zone submodel is solved using the Steffenson acceleration approach.

Two sets of experimental data for fire growth, including data for the post-flashover stage, have been used to validate the model's predictions. One set was for a standard test room, with the parameters of smoke layer temperature, interface height, and ventilation rate being compared. Another set was for an experimental atrium with a mechanical smoke exhaust system, where comparisons were made for the smoke layer temperature, smoke layer CO_2 concentration, and interface height. For all the compared cases, good agreement has been obtained. The validation work presented in this article is not meant to be comprehensive; when data are available, more validation work will be conducted.

NOMENCLATURE

A_V = vent area
A_w = surface area of a wall, ceiling or floor
b_P = combustion efficiency
C = specific heat
C_{E1}, C_{E2} = coefficients in McCaffrey's plume entrainment correlation
C_{LOL} = lower oxygen limiting coefficient
C_V = coefficient of door/window type vent flow

h = heat transfer coefficient
H_U = gas enthalpy of upper layer
H_V = height of opening
$(\Delta H)_O$ = heat of combustion per unit mass of oxygen
K = conductivity
m = mass
$\dot{m}_{air}$ = air flow rate
m_{CO} = mass production of CO
m_{CO_2} = mass production of CO_2
$\dot{m}_e$ = mass entrainment rate
$\dot{m}_f$ = mass outflow rate of smoke in one-zone post-flashover model
m_{H_2O} = mass production of water
m_{O_2} = oxygen consumption from air in combustion
m_{PF} = mass of fuel pyrolysis
$m_{PF_{min}}$ = mass production of the minimal part of fuel
m_{soot} = mass production of soot
m_{TUCF} = mass of the total unburned combustible fuel
P = pressure
P_b = pressure difference at the bottom position
P_t = pressure difference at the top position
Q = heat release rate
Q_{ceil} = convection heat loss to ceiling surface
Q_{conv} = convection heat loss to a surface of a wall, ceiling or floor
Q_N = nominal heat release rate of the fuel
Q_R = window radiation loss
Q_W = wall heat loss
$\dot{S}_i$ = net energy gain rate of layer i as a source term
T = temperature
t = time
T_a = ambient temperature
T_{ad} = adiabatic ceiling jet temperature
T_{amb} = ambient air temperature
T_{ceil} = ceiling surface temperature
T_f = temperature of outflow smoke
T_g = smoke layer temperature
T_w = surface temperature of a wall, ceiling or floor
V = volume
V_H = volumetric flow rate from high to low-pressure side
V_L = volumetric flow rate from low to high-pressure side
V_N = net volumetric flow rate
Y_{O_2} = oxygen mass fraction
Z_e = plume entrainment height

GREEK SYMBOLS

ρ = density
γ = ratio of specific heats
ϕ = equivalence ratio
$\dot{\Omega}_i$ = net mass gain rate of layer i by mass flow through its boundary
ω = coefficient used in plume entrainment for wall and corner fires

REFERENCES

1. Yung, D. and Beck, V.R., "Building Fire Safety Risk Analysis. SFPE Handbook of Fire Protection Engineering," National Fire Protection Association, Quincy, MA, 1995, pp. 5–95.
2. Yung, D., Hadjisophocleous, G.V. and Proulx, G., "Modeling Concepts for the Risk-cost Assessment Model FiRECAM and its Application to a Canadian Government Office Building," In: Proceedings of the Fifth International Symposium on Fire Safety Science, Melbourne, Australia, 1997, p. 619.
3. Takeda, H. and Yung, D., "Simplified Fire Growth Models for Risk-cost Assessment in Apartment Buildings," Journal of Fire Protection Engineering, Vol. 4, 1992, p. 53.
4. Fu, Z. and Hadjisophocleous, G., "A Two-zone Fire Growth and Smoke Movement Model for Multi-compartment Buildings," Fire Safety Journal, Vol. 34, 2000, p. 257.
5. Babrauskas, V. COMPF2: A Program for Calculating Post-flashover Fire Temperatures, National Bureau of Standards, NBS Technical Note 991, 1979.
6. Friedman, R., "An International Survey of Computer Models for Fire and Smoke," Journal of Fire Protection Engineering, Vol. 4, 1992, p. 81.
7. Olenick, S.M. and Carpenter, D.J., "An Updated International Survey of Computer Models for Fire and Smoke," SFPE Journal of Fire Protection Engineering, Vol. 13, 2003, p. 87.
8. Jones, W.W. and Forney, G.P., "Improvement in Predicting Smoke Movement in Compartment Structures," Fire Safety Journal, Vol. 21, 1993, p. 269.
9. Forney, G.P. and Moss, W.F., "Analyzing and Exploiting Numerical Characteristics of Zone Fire Models," Fire Science and Technology, Vol. 14, 1994, p. 49.
10. Schifiliti, R.P., "Design of Detection Systems," In: SFPE Handbook of Fire Protection Engineering, Third Edition, Section 4, Chapter 1, Society of Fire Protection Engineers, Bethesda, MD, 2002.
11. Bukowski, R.W., "A Review of International Fire Risk Prediction Methods, Interflam' 93," the 6th International Fire Conference, Oxford, England, 1993, p. 437.
12. Dembsey, N.A., Pagni, P.J. and Williamson, R.B., "Compartment Near-field Entrainment Measurements," Fire Safety Journal, Vol. 24, 1995, p. 383.
13. McCaffrey, B.J., "Momentum Implications for Buoyant Diffusion Flames," Combustion and Flame, Vol. 52, 1983, p. 149.
14. Mowrer, F.W. and Williamson, R.B., "Estimating Room Temperatures from Fires along Walls and in Corners," Fire Technology, Vol. 23, 1987, p. 133.
15. Peacock, R.D., Forney, G.P., Reneke, P., Portier, R. and Jones, W.W., CFAST, the Consolidated Model of the Fire Growth and Smoke Transport, NIST Technical Note 1299, 1993.

16. Cooper, L.Y., "VENTCF2: An Algorithm and Associated FORTRAN 77 Subroutine for Calculating Flow Through a Horizontal Ceiling/Floor Vent in a Zone-type Compartment Fire Model," Fire Safety Journal, Vol. 28, 1997, p. 253.
17. ASHRAE Handbook, Equipment Volume, Section 1, Chapter 3, American Society for Heating, Refrigerating and Air Conditioning Engineers, 1979, pp. 3.1–3.12.
18. Kreith, F., Principles of Heat Transfer, Third Edition, Intext Educational Publishers, New York, 1973, ISBN 070022422X.
19. Holman, J.P., Heat Transfer, 7th Edition, McGraw-Hill, New York, 1990, ISBN 0079093884.
20. Cooper, L.Y. and Woodhouse, A., "The Buoyant Plume-driven Adiabatic Ceiling Temperature Revisited," ASME Journal of Heat Transfer, Vol. 108, 1986, p. 822.
21. Motevalli, Y. and Ricciuti, C., Characterization of the Confined Ceiling Jet in the Presence of an Upper Layer in Transient and Steady-state Conditions, NIST-GCR-92-613, 1992.
22. Forney, G.P., "Analyzing and Exploiting Numerical Characteristics of Zone Fire Models," Fire Science and Technology, Vol. 14, 1994, p. 49.
23. Rehm, R.G. and Forney G.P., A Note on the Pressure Equations used in Zone Fire Modeling, NISTIR-4906, 1992.
24. Petzold, L., "Automatic Selection of Methods for Solving Stiff and Nonstiff Systems of Ordinary Differential Equations," Siam J. Sci. Stat. Comput., Vol. 4, 1983, p. 136.
25. Mathews, J.H., Numerical Methods for Mathematics, Science, and Engineering, Prentice Hall, Englewood Cliffs, NJ, 1992, ISBN 0136249906.
26. Dembsey, N.A., Pagni, P.J. and Williamson, R.B., "Compartment Fire Experiments: Comparison with Models," Fire Safety Journal, Vol. 25, 1995, p. 187.
27. Lougheed, G. and Hadjisophocleous G., Investigation of Atrium Smoke Exhaust Effectiveness, ASHRAE Annual Meeting, Boston, 1997.